

Thermoacoustic Stabilization of a Sequential Combustor with Ultra-low-power Nanosecond Repetitively Pulsed Discharges

Bayu Dharmaputra*, Sergey Shcherbanev, Bruno Schuermans, Nicolas Noiray*

CAPS Laboratory, Department of Mechanical and Process Engineering, ETH Zürich, 8092, Zürich, Switzerland

Abstract

This study demonstrates the stabilization of a sequential combustor with Nanosecond Repetitively Pulsed Discharges (NRPD). A constant pressure sequential combustor offers key advantages compared to a conventional combustor, in particular, a higher fuel flexibility and a wider operational range. However, thermoacoustic instabilities remain a barrier to further widen the operational range of these combustors. Passive control strategies to suppress these instabilities, such as Helmholtz dampers, have been used in some industrial systems thanks to their simplicity in terms of implementation. Active control strategies are however not found in practical combustors, mainly due to the lack of robust actuators able to operate in harsh conditions with sufficient control authority. In this study, we demonstrate that thermoacoustic instabilities can be suppressed by using a non-equilibrium plasma produced with NRPD in a lab-scale atmospheric sequential combustor operated at 73.4

*Corresponding authors

Email addresses: bayud@ethz.ch (Bayu Dharmaputra), noirayn@ethz.ch (Nicolas Noiray)

kW of thermal power. We employ continuous NRPD forcing to influence the combustion process in the sequential combustor. The two governing parameters are the pulse repetition frequency (PRF) and the plasma generator voltage. We examine the effect of both parameters on the acoustic amplitude, the NO emissions, and the flame centre of mass. We observe that for some operating conditions, with plasma power of 1.1 W, which is about 1.5×10^{-3} percent of the thermal power of the flames, the combustor can be thermoacoustically stabilized. By increasing the power of the plasma, the acoustic amplitude can be further reduced, at a small cost of a very low increase of NO emission. However, an additional increase in plasma power to 81 W, which is 1.1×10^{-1} percent of the flame thermal power, increase the NO emission significantly without significant improvement on the acoustic amplitude reduction. Furthermore, for some combinations of the plasma parameters, another thermoacoustic mode of the combustor at a different frequency can become unstable. This finding motivates further research on the optimization of the plasma parameters as a function of the thermoacoustic properties of the combustor where it is applied. This study is a pioneering effort in controlling the thermoacoustic stability of turbulent flames with plasma discharges at such low power compared to the thermal power of the sequential combustor.

Keywords: Thermoacoustic, Plasma Assisted Combustion, Control, Sequential Combustor

Novelty and significance

In this study, we demonstrate that Nanosecond Repetitively Pulsed Discharges (NRPD) can be used as an actuator to stabilize a thermoacoustically unstable sequential combustor. We suppress instabilities with a mean plasma power that is 5 orders of magnitude lower than the flames thermal power, i.e. more than 2 orders of magnitude lower than the current state of the art. This achievement therefore opens the door for commercial application of such a technology for continuous operation. Furthermore, we examine the impact of varying plasma parameters, specifically the plasma repetition frequency and generator voltage, on flame topology changes, as well as investigate the resulting NO emissions.

Authors contributions

B.D. led the experimental investigations and designed the analyses. B.D. and S.S. performed the experiments and analysed the data. N.N. conceived the research idea. B.D., S.S., B.S. and N.N. discussed the results. B.D. drafted the manuscript with the support of N.N. The final version of the manuscript has been edited and approved by B.D., S.S., B.S. and N.N.

1. Introduction

Gas turbines have played a significant role in global energy production. However, with the increasing proportion of renewable energy production and tightening emission restrictions, gas turbines now face new challenges, and in particular the need for fuel flexibility, fast ramp-up times, and a wide operational range [1]. One major technological breakthrough of the recent past

in gas turbine technologies is the constant pressure sequential combustor (CPSC) [2, 3]. It significantly improves the operational range with very low pollutant emissions, and the fuel flexibility, which is the ability to be supplied with blends of hydrogen and natural gas, as well as non-conventional fuels derived from waste processes or biomass gasification [1]. Notably, the combustion of pure H_2 in an academic CPSC configuration has been investigated recently in [4]. In CPSC configurations, the hot products from the first-stage combustor are diluted with air bypassing the first-stage before the sequential fuel is injected. This combustor architecture reduces the temperature of the vitiated air flow at the inlet of the sequential stage in order to prevent too fast autoignition of the sequential fuel in poorly mixed conditions. Ensuring in this way a sufficient mixing time of the globally lean mixture of gas and vitiated air, the exothermal reactions of the autoignition process in the sequential stage occur in well-mixed conditions, and the NO_x emissions can thus be drastically reduced.

Much like a traditional combustor, CPSC combustors are also prone to thermoacoustic instabilities [5, 6]. Thermoacoustic instabilities are challenging problems in gas turbines for power and propulsion applications [7]. These instabilities can lead to high amplitude acoustic pressure oscillations which can induce vibrations causing structural damages and possibly flame flashback [8]. Hence, developing technologies for controlling the instabilities is essential for the safety and operability of gas turbines. In the past decades, both active and passive control strategies have been investigated in academic and industrial laboratories and implemented in real engines. Nonetheless, gas turbine manufacturers usually opt for passive control strategies which

are more cost-effective so far.

Indeed, passive damping strategies have been widely studied and applied in real combustors. For example, the nonlinear behavior of Helmholtz resonators mounted on combustion chamber walls has been investigated in a recent study in order to draw design guidelines for avoiding failures of their damping effectiveness [9]. Furthermore, dampers based of interconnected cavities with broadband acoustic absorption capabilities were successfully implemented in large modern gas turbines [10, 11]. However, the design of these passive dampers is still challenging for the following two reasons: First, it requires costly engine testing for obtaining a relatively precise prior knowledge of the difficult-to-predict thermoacoustic instabilities, in order to tune their geometry for effective reduction of the acoustic amplitude. Second, for a given volume constraint for their implementation, there is always a trade-off to find between their broadbandness for addressing multiple instability frequencies and their effectiveness at a given frequency.

In contrast, active control strategies can adapt to the operating conditions of the system but, so far, their implementation in real engines has been hindered by the harsh thermodynamic and thermochemical conditions and by the lack of cost-effective and mechanically-robust actuation solutions. The big challenge of implementing active control strategies is thus finding suitable actuators [12, 13]. For example, the use of loudspeakers to stabilize an unstable combustor by tailoring its acoustic boundary conditions was successfully achieved in an academic configuration operated at atmospheric pressure [14] but could not be applied in a real engine. Another active control strategy, based on the fast modulation of the fuel mass flow has been

successfully developed about thirty years ago for liquid spray [15] and natural gas [16]. The latter technology has even been validated in heavy duty gas turbines and was commercialised. Nonetheless, effective modulation the pilot gas massflow cannot be achieved beyond 500 Hz, which prevents from addressing the problem of high-frequency instabilities with the corresponding valves. Furthermore, such modulation of the fuel massflow could negatively impact the pollutant emissions.

In this context, the search of alternative actuators for gas turbine combustors, with high control authority, low power consumption, and minimal additional emissions is highly relevant for increasing fuel and operational flexibility of future gas turbines. In this work, we focus on ultra-low-power plasma actuation, which has never been implemented in industrial systems so far, and we show that it is a very promising strategy for suppressing thermoacoustic instabilities in sequential combustors without increasing NO_x emissions.

Non-equilibrium plasma discharges can be used to enhance combustion reactions through thermochemical effects [17, 18, 19, 20, 21]. In these plasmas, the substantial difference between electron and gas temperatures ($T_e \gg T_{gas}$) results in the efficient formation of active species and radicals through direct electron impact, which can help to ignite combustible mixtures, and to extend lean flammability limits [22, 23, 24].

Owing to its high influence to the kinetics of the reactive mixture, several studies have been performed to characterize the effect of nanosecond repetitively pulsed discharges (NRPD) on the heat release rate oscillations of acoustically-forced flames. For instance, Lacoste et al. [25] have studied

this effect in a single stage swirled stabilized combustor. It was shown that NRPD affects significantly the gain and phase of the flame transfer function (FTF) and thereby, might influence the thermoacoustic stability of the combustor. In [26], it was shown with a laminar flame that strong heat release rate modulation can be induced by periodic series of constant voltage NRPD. The forcing mechanism was mainly attributed to the increase of local burning velocity close to the plasma region. In a similar set-up to the one in [25], Moeck et al. [27] have successfully demonstrated the applicability of nanosecond plasma discharges to stabilize a linearly unstable combustor with active feedback control. By using the extended kalman filter (EKF), the instantaneous phase of the acoustic pulsation was estimated and then fed to the gate signal for the actuation of the plasma generator. The plasma power required to stabilize the combustor was at around 1 percent of the flame thermal power. Furthermore, Kim et al [28] have demonstrated the capability of NRPD to stabilize a combustor at realistic low power condition of aero-engine combustors.

Nanosecond plasma discharges in pin-to-pin configuration have shown high potential for second-stage flame stabilization in constant-pressure sequential combustors, as the hot reactive mixture in the sequential burner already undergoes radicals-producing chemical reactions that precede auto-ignition. Xiong et al. [29] demonstrated that NRPD could shorten significantly the auto-ignition time of a CH_4 sequential flame with low electric power and NO emissions. In a more compact laboratory-scale sequential combustor, Shcherbanev et al. [30] demonstrated the effectiveness of plasma discharges in igniting very lean mixtures of hydrogen and natural gas, and

therefore could help keeping the sequential flame alive. One significant advantage of the NRPD actuation is that the electrode system implementation does not require a drastic modification of the combustor geometry and could also be considered for retrofitting existing systems.

Another advantage of NRPD is their fast response time, which enables high frequency actuation without moving parts that are usually causing reliability and durability issues in mechanical actuators. Indeed, non-equilibrium plasma actuation can quickly influence flames, improving their stability and extending their lean flammability limit [31, 32].

Finally, the mean NRPD power is known to be small compared to the thermal power of the flame [33, 31, 25]. It should be noted that the mean NRPD power reported in literature pertains only to the electrical energy that gets transferred to the system, without accounting for the electrical energy necessary for the high voltage generator. However, if we consider an optimistic scenario where an exceptionally efficient high voltage generator is feasible, including the achievement of a perfect impedance matching at the electrodes, the generator's power requirements would match the energy deposited into the system. In the case of a sporadic use of the NRPD, for flame ignition assistance or during transient operation, the electric power requirements of a NRPD system is not a major driver in the development of plasma assisted combustion technologies. Although the mean NRPD electric power reported in previous works is of the order of 1 percent of the thermal power of the flame [27, 34], it is worth mentioning that the cost-benefit analysis of a NRPD system with an electric power of 1 percent of the combustor thermal power would not be straightforward for heavy duty gas

turbines, for the following two reasons. First, 1 percent is still a large penalty for gas turbine manufacturers which struggle for gaining any 0.1 percent of engine thermal efficiency during stationary operation (over the last decade, this efficiency increased toward 65 percent for combined cycle power plants by only a couple of percents). Second, for an H-class gas turbine exhibiting a combustor with 1 GW of thermal power, it means that, by assuming linear scaling, a system of 10 MW electric power would have to be developed, just for the NRPD actuation, which is technically rather challenging. In the present work, we demonstrate that for a sequential combustor, operated at atmospheric pressure, successful actuation suppressing thermoacoustic instabilities can be achieved with a mean plasma power that is about 3 orders of magnitude lower than 1 percent of the thermal power, which would be much more realistic for implementation in practice (for 1 GW of thermal power, one would need about 10 kW of mean plasma power). Therefore, as research in this area continues, it is foreseen that such NRPD technology may be implemented in future gas turbines burning green H_2 in sequential combustors for compensating the intermittency of renewable sources.

This study thus aims at introducing the ultra-low-power nanosecond plasma rapid discharges (NRPD) to thermoacoustically stabilize a sequential combustor which had never been attempted so far. Additionally, parametric studies on the plasma repetition frequency (PRF) and the generator voltage are performed to investigate the effectiveness of the actuator in suppressing the instability and the associated NO emissions.

2. Experimental Setup

The lab-scale sequential combustor is depicted in figure 1. The setup consists of a plenum, a 4×4 array of jet flames anchored on a so-called matrix burner, a combustion chamber with $62 \times 62 \text{ mm}^2$ cross section, a dilution air section, a sequential burner featuring a mixing channel with $25 \times 38 \text{ mm}^2$ cross section in which secondary fuel is injected, a sequential or second-stage combustion chamber equipped with a motor-driven adjustable outlet orifice. This variable outlet geometry enables an online tuning of the acoustic reflection coefficient, and thus an independent control of the thermoacoustic instabilities, which is key for validating the NRPD-based control. The first stage combustor is fed with a mixture of natural gas and air, with the air preheated to 230 C and supplied from the plenum, while natural gas is added in the matrix burner, which corresponds to a technically premixed first stage. The thermal power of the first stage combustor is 35 kW with an equivalence ratio of 0.7. A piezo sensor is placed on a flush mounted plate to monitor the acoustic pressure inside the first stage and denoted as Mic. 1 in the figure. A massflow of 18 g/s of dilution air at 25 C is introduced from the dilution air port and mixes with the hot gases from the first stage. A mixture of 0.07 g/s of hydrogen and 0.6 g/s of natural gas is injected into the sequential injector. The sequential injector features an X-shaped vortex generator to enhance the mixing process. The total thermal power of the two flames is 73.4 kW. A pin-to-pin electrode configuration, with an inter-electrode distance of 5 mm, is located 10.3 cm downstream from the sequential fuel injector, and a gas analyzer (ABB-EL3040) probe is placed at 45 cm from the outlet of the second-stage burner to monitor the NO emissions. Another piezo sensor is

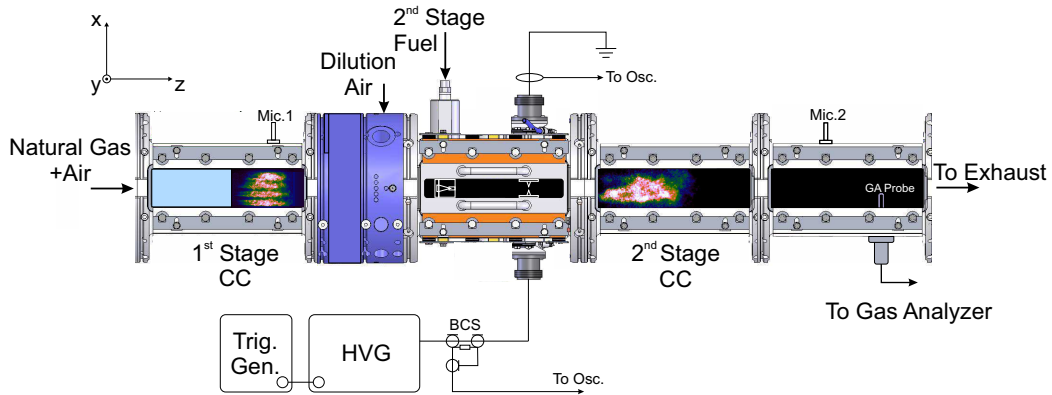


Figure 1: Lab-scale sequential combustor test-rig. CC- Combustion chamber, HVG- High Voltage Generator, BCS- Back Current Shunt.

placed downstream of the sequential flame to monitor the acoustic pressure in the second combustion chamber. As indicated above, the outlet of this chamber has an adjustable orifice to control the thermoacoustic stability.

The OH^* chemiluminescence is used to characterize the sequential flame, with the camera capturing a portion of the mixing channel downstream of the electrodes. The intense light emission from the plasma discharges is masked by an optical obstacle. The recording setup comprises of a LaVision Star X high-speed CMOS Camera and a LaVision HS-IRO high-speed intensifier, which are equipped with a 45 mm CERCO UV lens (F/1.8 Cerco) and an Edmund Optics optical bandpass filter (centered at 310 nm, FWHM 10nm).

To measure the energy deposition of the plasma, a current probe and a back current shunt are placed on the anode and cathode to acquire current and voltage. The plasma generator (FID) initiates the high voltage pulses with a 2-3 ns rise time and a pulsed width of 10 ns. A mixed signal digital oscilloscope (Tektronix MDO3104) was used to record the current and the

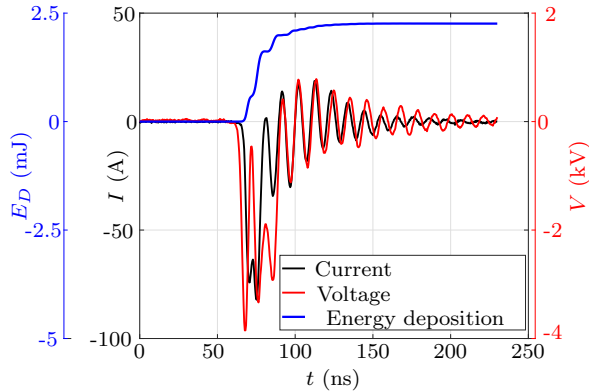


Figure 2: Waveforms of current (black), voltage (red), and energy deposition (blue) . The energy deposition is obtained by taking the integral of the product of the current and voltage signal. The measured voltage corresponds to the voltage across the electrodes' gap and hence it is not necessarily equal to the voltage of the generator.

voltage signals at 1 GHz bandwidth and 5 GHz sampling rate. A Pearson fast current monitor (model 6585, 0.5 V/A, 50.) was used to measure the current. During testing, four generator voltages (11, 11.7, 12.5, and 14 kV) at three pulse repetition frequencies (10, 20, 40 kHz) were used, with an additional voltage value of 13.2 kV at 40 kHz. All experiments were performed using only the negative polarity of applied pulses.

The energy deposition measurement of a single pulse for continuous NRPD at 14 kV and 10 kHz is shown in figure 2. Note that due to the mismatch between the generator impedance and the plasma impedance, oscillations in voltage and current are observed. The deposited energy is computed by taking the time integral of the product of voltage and current. At this condition, mean energy deposition is around 2 mJ per pulse. The type of plasma at this energy is classified as spark plasma [35]. The resulting energy deposition at

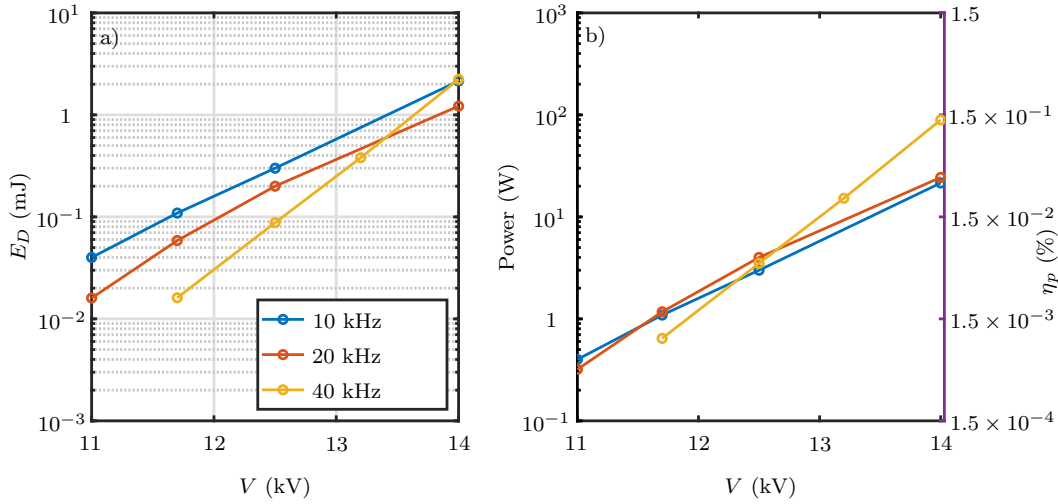


Figure 3: Energy deposition measurement a) and the plasma power b) at three different PRFs and four generator voltages. The mean plasma power is obtained by taking the product of the PRF and the energy deposition. The ratio between the mean plasma power and the thermal power of the combustor is indicated on the right y-axis in b). There is no plasma discharge observed at PRF =40 kHz and $V = 11$ kV.

all conditions are shown in figure 3a. It is interesting to note that the y-axis has a logarithmic scale, and that the energy deposition increases exponentially with respect to the generator voltage. Furthermore, except at 14 kV, the energy deposition per pulse at higher frequency and at the same voltage decreases. This is probably due to the interference between the incoming and reflected pulses inside the high voltage cable. Furthermore, there was no plasma observed at 11 kV and 40 kHz and consequently the data can not be shown in the plot.

By multiplying the energy deposition and the plasma repetition frequency (PRF), the mean plasma power is obtained and depicted in figure 2b. The highest power is at 81 W which amounts to 1.1×10^{-1} percent of the thermal

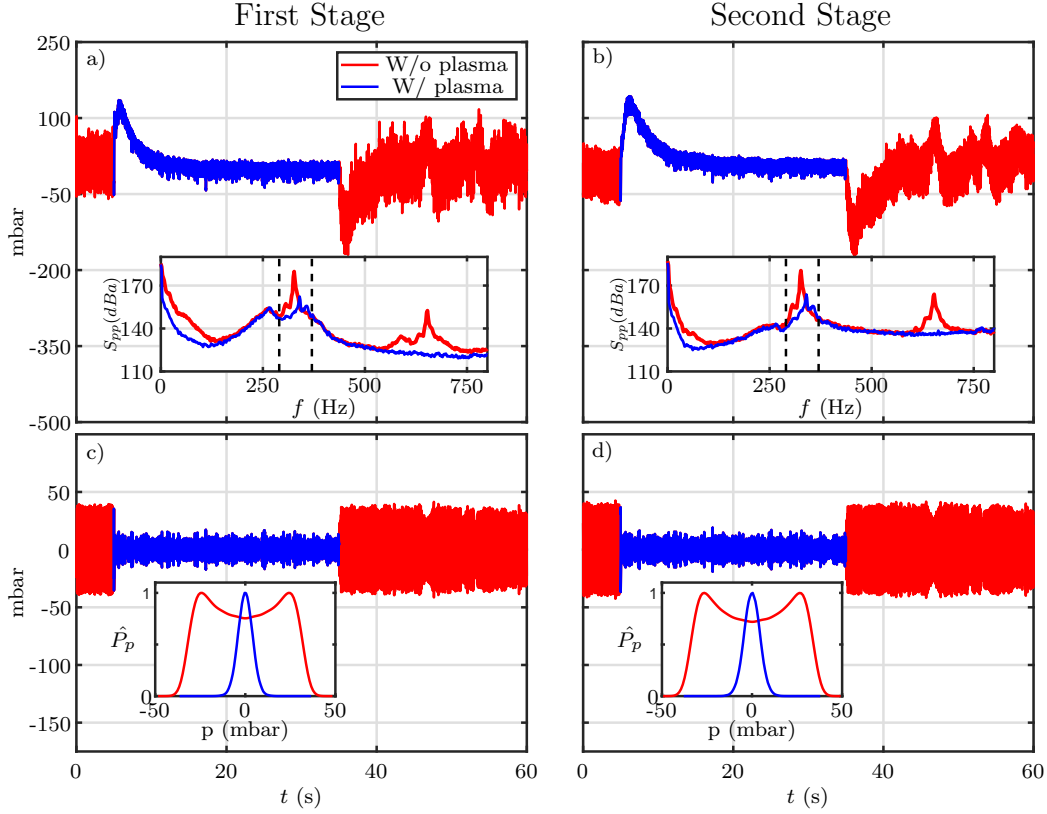


Figure 4: The time trace of the acoustic pressure signal with and without plasma discharges and their corresponding power spectral density inside the first a) and second b) stage combustion chambers. The PRF is at 10 kHz and the generator voltage is at 11.7 kV, the mean plasma power is 1.1 W, which is about 1.5×10^{-3} percent of the thermal power of the flame. The bandpass filtered acoustic pressure signal and its associated normalized probability density function inside the first c) and second d) stage combustion chambers. The low-pass and high-pass frequency are indicated by the dashed lines in a) and b).

power of the flames. The ratio between the plasma to thermal power is indicated on the right axis of the figure 3b) which we denote as η_p .

3. Results

Figure 4 shows the effects of plasma discharges on the stability of the sequential combustor at a PRF of 10 kHz and generator voltage of 11.7 kV. The plasma was turned on at $t = 5$ s and turned off at $t = 35$ s. In Figure 4a and 4b, the acoustic pressure signals from the first and second stage combustion chambers are presented, along with their corresponding power spectral density. Without plasma discharges, the combustor exhibits a strong pulsation at the frequency of 330 Hz, by looking at the corresponding probability density of the bandpass filtered time trace around 330 Hz, it is clear that the system exhibits a stable limit cycle. Furthermore, the power spectral density of the first microphone show a resonance peak at 260 Hz. It is worth mentioning that the thermoacoustic instability can alternatively be suppressed by adjusting the outlet orifice area at the considered operating point.

Immediately after the start of the plasma actuation, a burst of the mean value of the unfiltered dynamic pressure signal is observed and then decay within a few seconds. This burst is attributed to the rapid change of flame position induced by the start of the NRPD, and a presumed abrupt variation of the pressure drop across the sequential burner. Nevertheless, its amplitude and relaxation time do not provide quantitative information about the actual evolution of the mean pressure in the combustor because the piezoelectric sensor signal is high-pass filtered in the data acquisition system. The purpose of this work is the study of thermoacoustic stability control with NRPD. Therefore, the acoustic signals are bandpass filtered around the thermoacoustic peak frequency of 330 Hz and are shown in Figure 4c and 4d, together with their corresponding scaled probability density

functions (PDFs) in the inset.

As it can be seen in figure 4c and 4d, when the plasma is on, the combustor becomes linearly stable. In contrast, without the plasma, the PDF of the acoustic pressure exhibits a bimodal distribution which is a typical feature of a system undergoing a limit cycle. Additionally, the first harmonic at around 660 Hz is also observed in the power spectral density.

Figures 5a to 5f show the OH chemiluminescence of the sequential chamber and of a portion of the burner mixing channel. In figures 5a to 5c, the OH chemiluminescence is shown at three different time instances before plasma initiation, while figures 5d to 5f show the OH chemiluminescence after plasma activation. The PRF is at 10 kHz with a generator voltage of 11.7 kV. The mean intensity within the red and blue squares in figures 5a to 5f is illustrated in figure 5g. Figure 5h depicts the acoustic pressure inside the first and sequential combustion chambers. Remarkably, the thermoacoustic limit cycle in the sequential combustor can be effectively suppressed with a mean plasma power of only 1.1 W, which is about 1.5×10^{-3} percent of the thermal power of the flame. The mean plasma power in our case is similar to that in [34]; however, the thermal power of the flame in our case is 300 times higher than that in their case.

In Figure 6, the frequency spectra of the pressure oscillations are displayed, with the PRF fixed at 10 kHz and at varying generator voltages. It is evident that the peak corresponding to a limit cycle around 330 Hz becomes smaller, and thus corresponding to a thermoacoustic stabilization, and shifts to higher frequencies as the voltage and energy deposition increase. This frequency shift can be indirectly attributed to a change in the mean

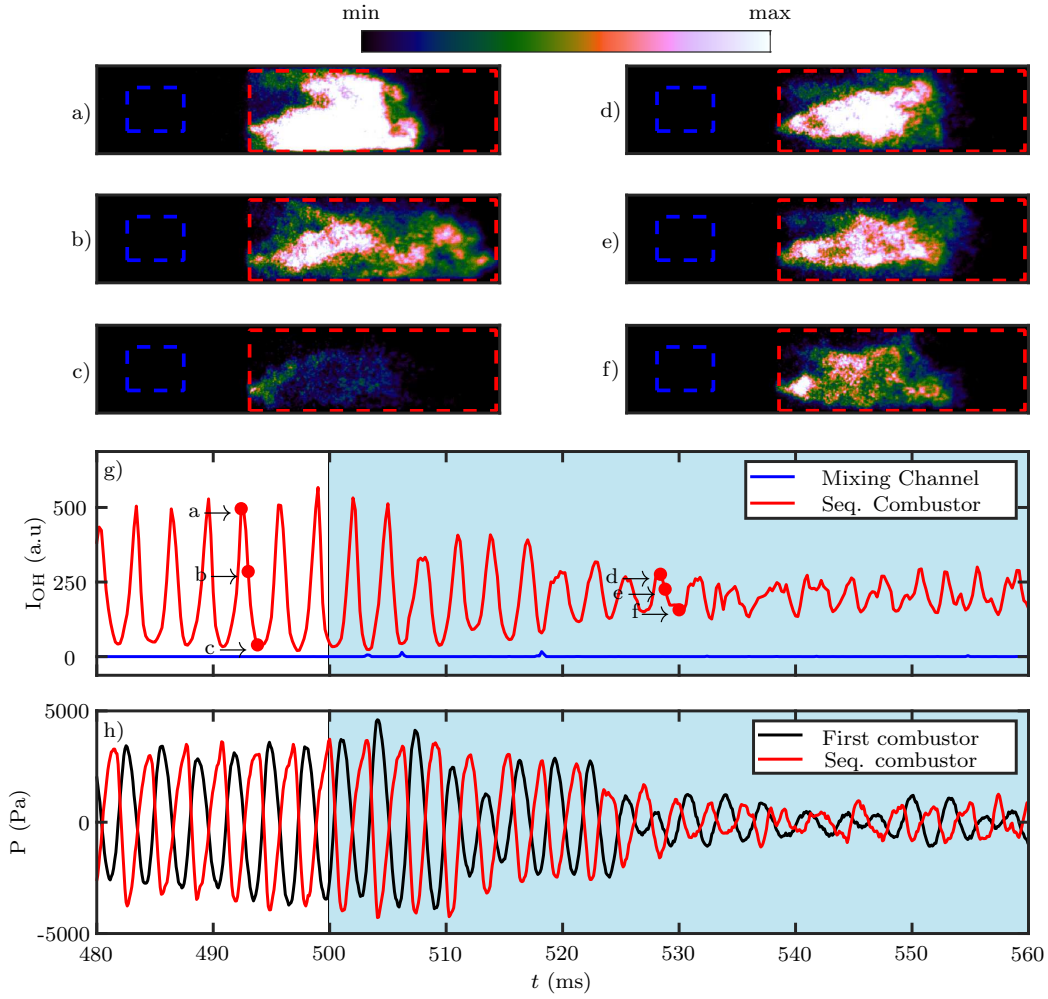


Figure 5: (a-f) OH chemiluminescence of the sequential combustor at 6 different time instances with the time instances shown in g). The PRF is 10 kHz and the generator voltage is 10 kV. Plasma is initiated at $t = 500$ ms. g) The mean OH intensity inside the mixing channel and sequential combustor. h) The bandpass filtered acoustic pressure signal inside the first and sequential combustor.

flame position, which will be quantified later. In Figure 6a, another peak at around 260 Hz becomes more prominent as the voltage is increased, but

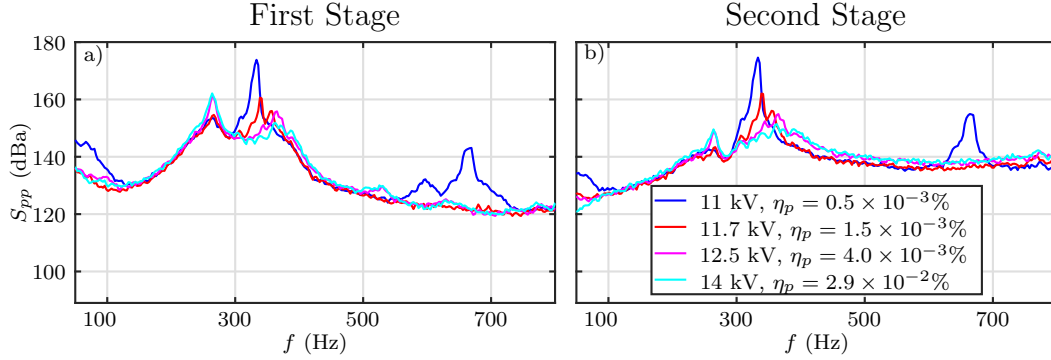


Figure 6: The frequency spectra of the acoustic pressure signal with plasma discharges at PRF = 10 kHz and four different generator voltages inside the a) first and b) second stage combustor.

the gaussian-like PDF of the acoustic pressure filtered around that peak (not shown here), indicates that it remains a resonance peak, i.e. the thermoacoustic oscillations at that frequency are linearly stable. Notably, the first microphone has a more intense peak around 260 Hz compared to the second microphone. However, for the mode at 330 Hz, almost the same amplitudes are observed with both microphones.

Another important aspect of the actuator’s performance is its ability to stabilize the system quickly, which can be expressed as a decay rate. To measure this decay, in a similar way as in [36], a periodic on-off cycle of plasma actuation is applied. The plasma is turned on for 5 seconds, followed by a 5-seconds off period, and the entire cycle is repeated for 5 minutes. The time trace of the first microphone’s bandpass-filtered acoustic signal during this process is shown in Figure 7, with the PRF set at 10 kHz and the generator voltage at 12.5 kV. The envelope of the acoustic pressure signal A is obtained from this data by computing the analytical signal using the

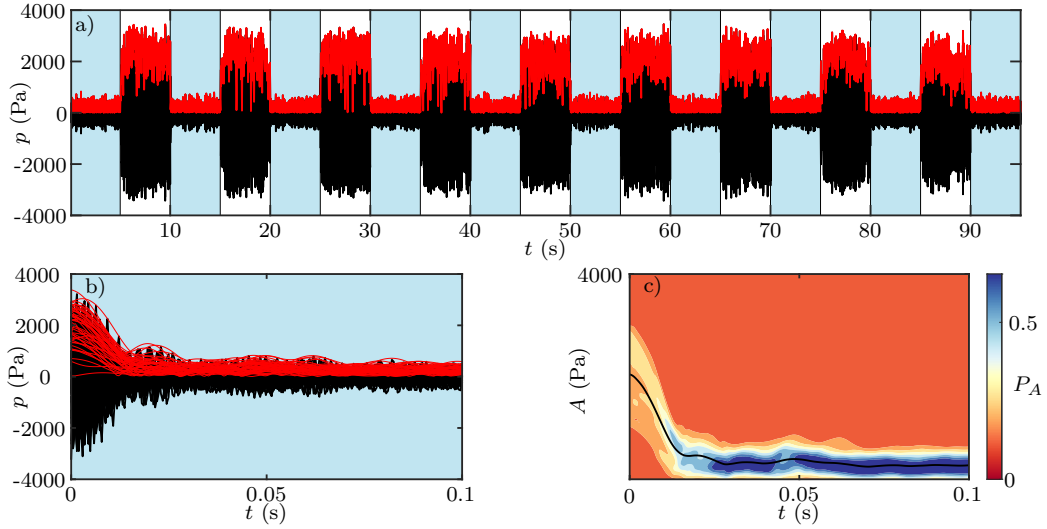


Figure 7: a) Periodic on-off plasma excitation at PRF = 10 kHz and generator voltage of 12.5 kV, the modulation frequency is at 0.1 Hz, red and black line depict the envelope and acoustic pressure evolution, respectively. The blue shaded regions show the period in which the plasma is on. b) Cycle to cycle superposition of acoustic pressure time trace. c) The time evolution of the distribution of the acoustic pressure envelope A is shown for the first 0.1 second of the actuation. The mean envelope \bar{A} is the black line.

Hilbert transform, and it is averaged over the cycles. Figure 7 illustrates the distribution of the pressure envelope at different time points, with the black line indicating the mean value. This procedure is repeated at generator voltages of 11.7 kV and 14 kV. The resulting decay rates at different voltages are shown in Figure 8, where the envelope is normalized to its value at $t = 0$ for better comparison. It is evident that the envelope decays faster as the voltage increases. The system takes around 30 ms to reach a quasi steady-state value with generator voltages of 12.5 and 14 kV, and the steady-state value is lower at higher voltages.

Figure 9 displays the time evolution of the flame centre of mass at PRF of

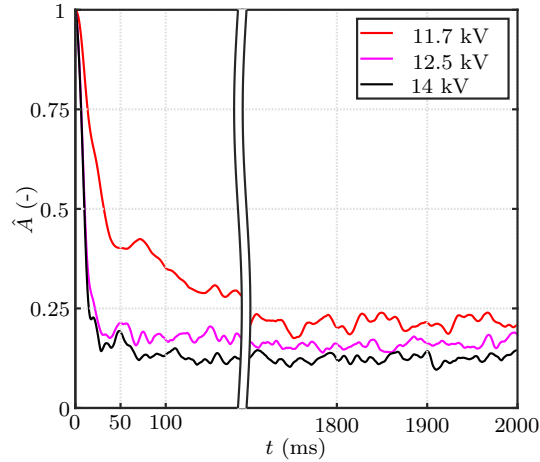


Figure 8: Evolution of the normalized mean acoustic pressure envelope after plasma is applied at three different generator voltages. The values of the envelope are normalized with respect to their value at $t = 0$ ms

10 kHz and various voltages. The OH^* chemiluminescence data are vertically integrated, and the centre of mass is computed along the streamwise direction. At 11 kV, the plasma has little effect on the flame, and the fluctuation around 330 Hz is still evident. With increasing voltage, the fluctuation of the flame centre of mass reduces more rapidly, which is strongly correlated with the pressure signal. Moreover, the steady-state value of the flame centre of mass with plasma actuation decreases as the voltage is increased, and the centre of mass shifts closer to the burner outlet. This shift is due to higher energy deposition, resulting in increased mean plasma power that enhances the autoignition process in the mixing section of the sequential burner more effectively.

Although the decay rate gets faster and the acoustic pressure amplitude gets smaller as voltage increases, NO emissions increase slightly. Figure 10

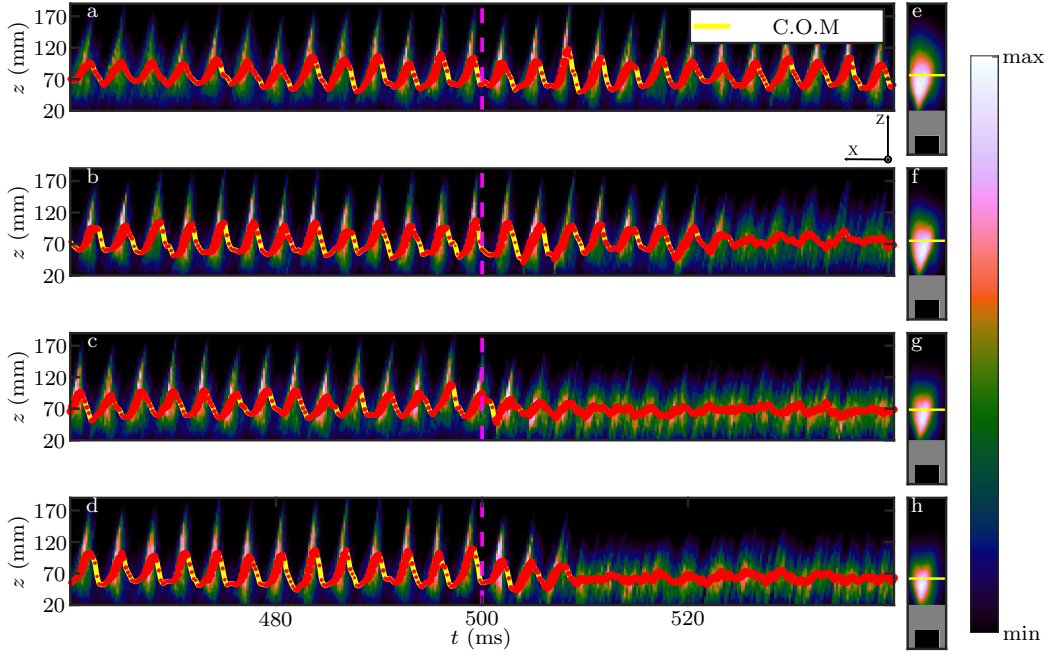


Figure 9: Evolution of the OH^* intensity integrated horizontally along the x -axis and the flame centre of mass before and after the plasma actuation (a-d). Only the region in the sequential combustor, which corresponds to the red box in figure 5, is considered. The start of the plasma actuation is at $t = 500$ ms and indicated by the dashed magenta line in (a-d). The size of the red markers is proportional to the sum of OH^* chemiluminescence intensity. The PRF is fixed at 10 kHz, the generator voltages are a) 11 kV, b) 11.7 kV, c) 12.5 kV, and d) 14 kV. The corresponding averaged flame OH^* chemiluminescence images after the plasma initiation for each generator voltage are presented in (e-h).

shows the root mean square of the acoustic pressure p_{rms} , NO emissions, and the flame center of mass with respect to generator voltage. As it can be seen, NO emissions increase from around 10 ppmvd at 11 kV to around 12 ppmvd at 14 kV. It is a well-known fact that spark plasma can produce

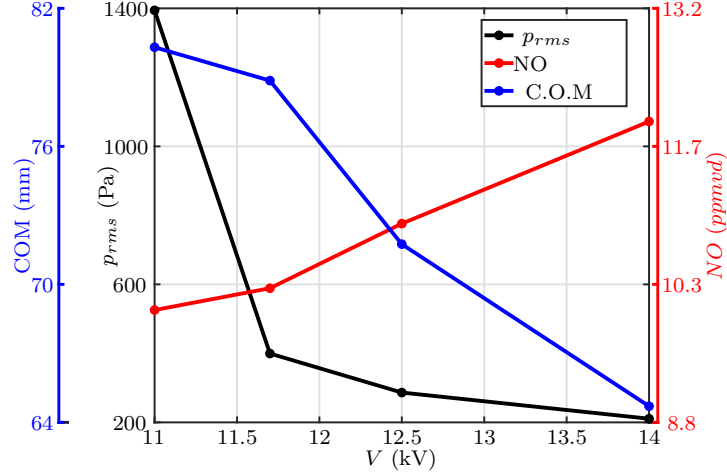


Figure 10: The dependency of root mean squared of acoustic pressure (band-pass filtered around 330 Hz), NO emission, and the flame centre of mass on the applied generator voltage. The PRF is fixed at 10 kHz.

significant NO emissions [37]. However, in our configuration, the flame center of mass is shifted upstream, resulting in an increased residence time for the burnt gases which can also be the cause of the NO increase. Furthermore, the energy deposition increases by an order of magnitude, from 0.2 mJ to 2 mJ, as depicted in figure 3. According to [30], the plasma regime changes from glow to spark. However, NO emissions only increase by less than 1 ppmvd. Therefore, the upstream shift of the flame centre of mass is suspected to be the dominant contributor to the increase in NO emissions. The exact mechanism behind this process is not yet clear, and further investigations are needed.

The same approach was followed at higher PRFs, and the resulting p_{rms} and NO emission maps are shown in figure 11. Since the thermoacoustic

peak of interest in the power spectral density of the acoustic pressure is at around 260 Hz, the bandpass filter was set to span from 200 Hz to 400 Hz for the rms calculation. Examining the map, we observe that at 11.7 kV, the plasma discharges at PRF = 10 and 20 kHz are more effective than that at PRF = 40 kHz. This is consistent with the fact that the mean plasma power obtained at 40 kHz for this voltage is lower than the one at 10 kHz or 20 kHz as shown in figure 3b. At 40 kHz and 11.7 kV, the plasma is thus not strong enough to affect the system. However, at 12.5 kV, all mean plasma powers at all PRFs are in the same order of magnitude (see figure 3b). When the PRF is set to 40 kHz, the rms pressure increases. The same behavior is observed at 13.2 kV, but the system is stabilized again when the voltage is set to 14 kV. Because there is a strong pulsation at $V = 13.2$ kV and PRF = 40 kHz, NO measurement could not be done. Nevertheless, it is clear that the NO emission map shows an increasing trends towards high PRF and high generator voltage, which is consistent with the findings in [29], which investigated the effect of plasma on the sequential flame position and on the NO emissions in another sequential combustor. By looking at the contour maps, it is evident that staying at PRF = 10 kHz with a pulse voltage above 11 kV, the thermoacoustic eigenmode in the combustor can be effectively stabilized without compromising the NO emissions. The dependency of NO emissions on the flame centre of mass and mean plasma power for all operating points will be further discussed in the subsequent paragraphs.

To shed light on the peculiar phenomenon at PRF = 40 kHz, it is interesting to show the power spectral density of both microphones. This information

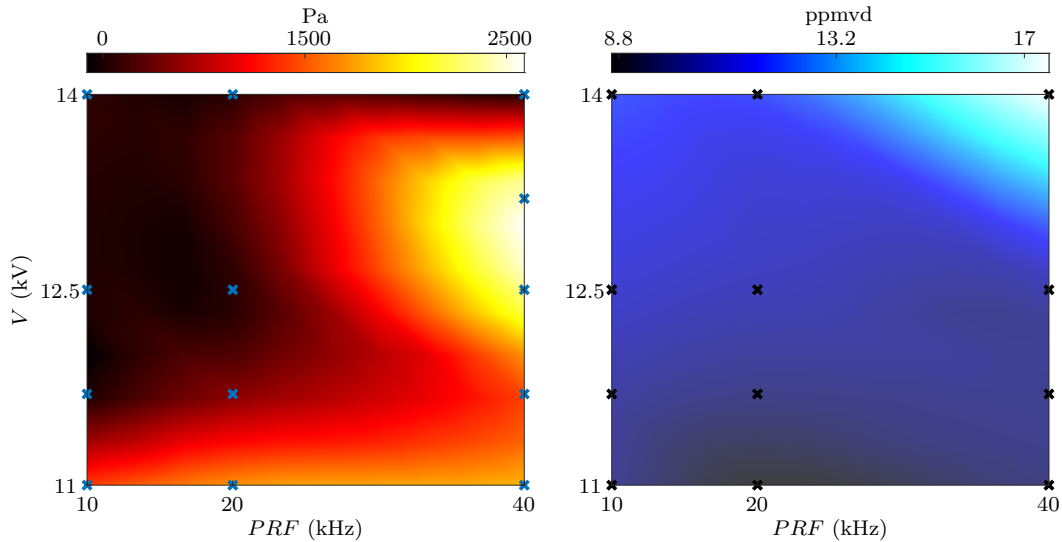


Figure 11: Contour maps of the rms acoustic pressure (left) and the NO emission (right) with respect to the variation of plasma repetition frequency and pulses voltage. The crosses indicate the measurement points. The bandwidth for the rms acoustic pressure calculation is from 200 Hz to 400 Hz. The NO measurement at $V = 13.2$ kV and $PRF = 40$ kHz is not available because the combustor cannot be operated for a long enough time interval at this condition due to excessive acoustic amplitudes.

is given in figure 12. Notably, at 12.5 kV and 13.2 kV, the mode at 260 Hz becomes self-excited and exhibits a very high amplitude of 180 dBa, while the mode at 330 Hz is stabilized. The PDF of the acoustic pressure \hat{P}_p shown in figure 12c exhibit in the case of repetitive pulses of 13.2 kV a typical feature of intermittently unstable thermoacoustic system. This observation is also confirmed by the time trace of the filtered signal. According to [38], such intermittent behavior can be caused by random fluctuations of the time delay of the flame response to acoustic perturbations around the mean time delay. For time delay fluctuations that can be described by an Ornstein-Uhlenbeck process, intermittent high amplitude bursts of oscillations occur when these

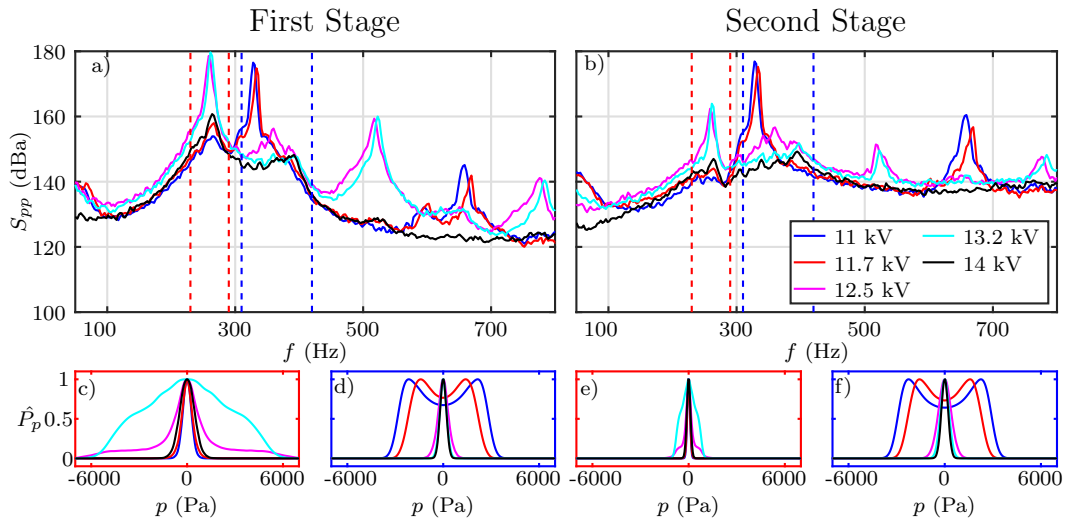


Figure 12: The frequency spectra of the acoustic pressure signal with plasma discharges at PRF = 40 kHz at four different generator voltages inside the a) first and b) second stage combustor. The acoustic pressure histogram of the bandpass filtered signal inside the first stage combustor at around 260 Hz c) and 330 Hz d). The acoustic pressure histogram of the bandpass filtered signal inside the second stage combustor at around 260 Hz e) and 330 Hz f). Another mode at around 260 Hz is excited when the generator voltage is at 12.5 kV and 13.2 kV.

fluctuations induce excursions of the system in linearly unstable conditions, and when the correlation time of the fluctuations is long enough to allow the thermoacoustic system to adapt to the random changes of stability [38]. In the present case, the fluctuating time history of the ignition kernels produced by the plasma could be the source of this time delay perturbation. However, to identify the exact reason for this behavior, further thermoacoustic analysis is required, which will be the subject of future investigations.

The OH chemiluminescence signals at 13.2 kV and PRF = 40 kHz, recorded during a time interval when the NRPD was activated, are shown

in figures 13a to 13f. When the NRPD actuation is turned on with these pulse generator settings, the thermoacoustic dynamics changes from a robust limit cycle at 330 Hz, to a limit cycle at 260 Hz, and in contrast with the PRF of 10 kHz and 20 kHz, the thermoacoustic system is not stabilized. As it can be seen in figure 13, OH chemiluminescence is visible inside the mixing channel after plasma actuation, due to the formation of ignition kernels induced by the NRPD. Figure 13g shows the OH chemiluminescence intensity inside the mixing channel, which fluctuates as the one in the combustion chamber at the acoustic pressure oscillation frequency of 260 Hz. The acoustic pressure time trace shown in figure 13h clearly indicates that, prior to plasma actuation, both microphones record similar acoustic pressure amplitudes. However, after the NRPD are applied, the acoustic pressure in the first stage combustor is significantly higher than that in the sequential combustor. This observation is consistent with figure 12, which shows a 20 dB difference in power spectral density at 260 Hz between the two microphones. It appears that the thermoacoustic mode at 260 Hz is more localized inside the first combustor than in the second combustor.

The plasma discharges are visualized in figure 14. The images are phase averaged with respect to the bandpass-filtered acoustic signals of the first microphone. As it can be seen, during an oscillation cycle, when the acoustic pressure in the first stage combustor reaches the maximum point, the plasma bends towards the outlet of the sequential burner. Whereas at the other phase angles, the discharge channels are relatively straight. The plasma bending effect is similar to the one observed in [30]. In this reference, the bending occurs because the inter-pulse time of the discharges is

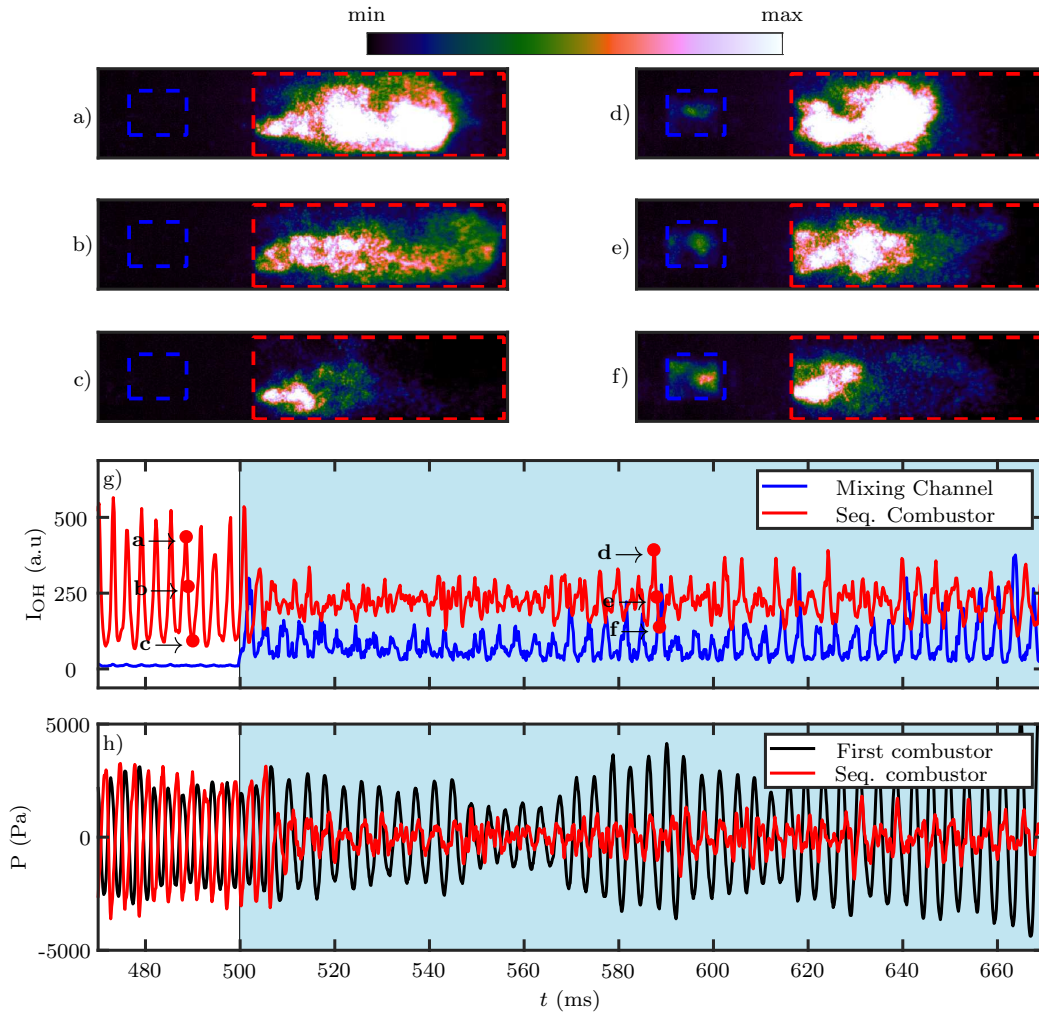


Figure 13: (a-f) OH chemiluminescence of the sequential combustor at 6 different time instances, the PRF is at 40 kHz and the generator voltage is at 13.2 kV. g) the mean OH intensity inside the mixing channel and sequential combustor. h) The bandpass filtered acoustic pressure signal inside the first and sequential combustor.

close to the convective time, but in contrast to the present work, there was no thermoacoustic instability at the considered operating conditions. In the present work, the thermoacoustic instability leads to the synchronization of

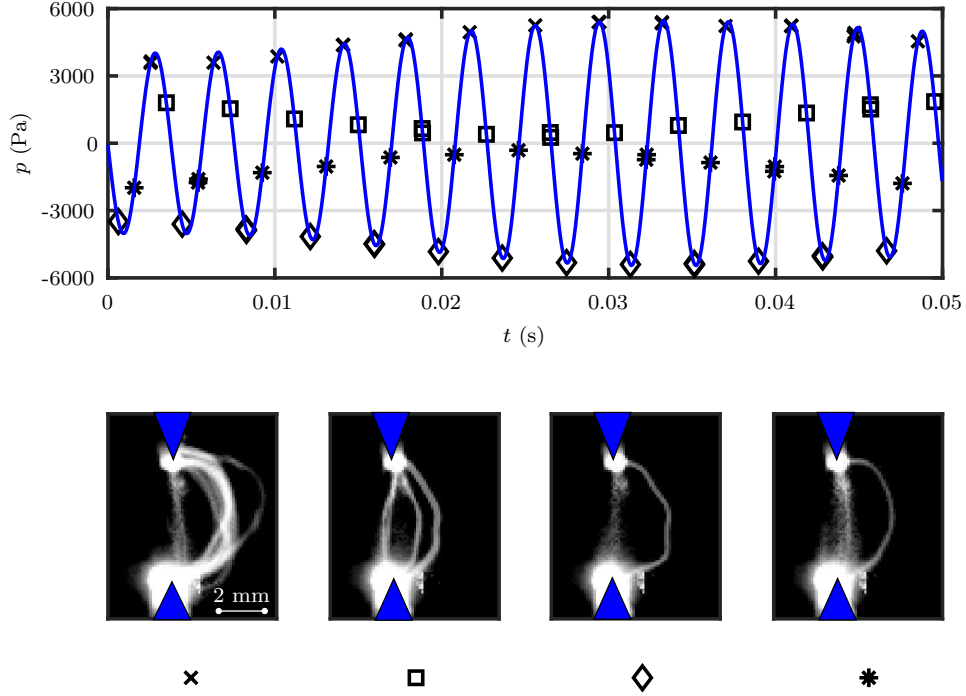


Figure 14: Phase average of the plasma discharge at $V = 13.2$ kV and PRF = 40 kHz (second row). The reference signal for the phase averaging is the microphone inside the first stage combustion chamber (first row).

the periodic plasma channel bending with the acoustic field.

Figure 15a shows the NO emissions of the combustor with different NRPD voltages and PRF, plotted against the relative distance between the emission probe location and the flame centre of mass. One measurement point without the plasma, which is indicated by a red cross in figure 15a, is obtained by stabilizing the combustor through adjusting the outlet orifice. The maximum NO emission of approximately 17.65 ppmvd occurs at a generator voltage of 14 kV and a PRF of 40 kHz, with a general increasing trend

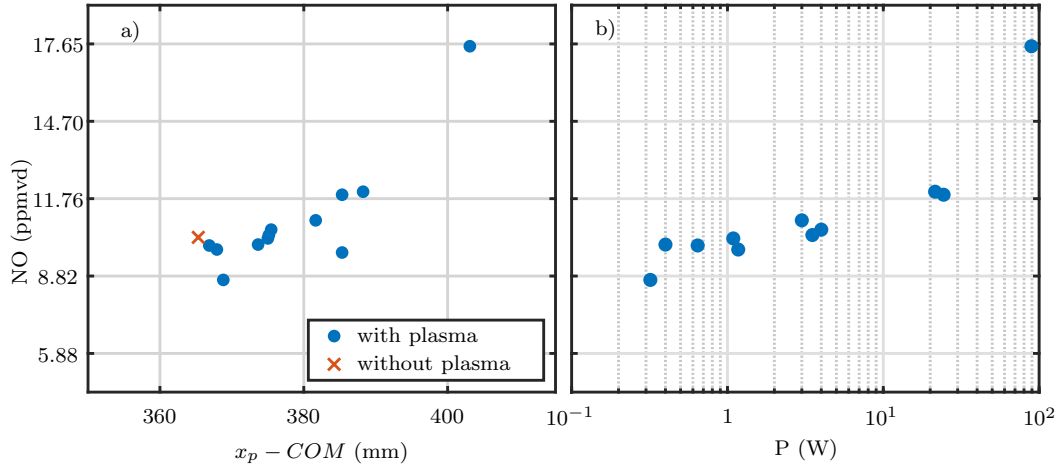


Figure 15: a) NO emissions as a function of the relative distance between the probe location and the flame centre of mass. The red cross is the NO measurement at thermoacoustically stable condition without plasma, obtained through adjusting the outlet orifice geometry. b) NO emissions as a function of the mean plasma power.

observed as the relative distance increases. It is worth noting that high PRF and voltage can cause early ignition inside the sequential burner mixing channel, leading to a reduction in mixing quality between the vitiated flow and the secondary fuel and consequently a potential increase in NO emissions. In Figure 15b, a weak correlation between NO emissions and mean plasma power is observed at power levels ranging from 0.1 to 10 W. However, as the mean plasma power increases to 20-81 W, a positive correlation is observed, potentially due to the residence time of the burnt gases or plasma-generated NO. Still, as the goal of the NRPD actuation in this work is to thermoacoustically stabilize the sequential combustor, a generator voltage of 11.7 kV and PRF of 10 kHz is obviously the optimum because the plasma does not lead to an increase of the NO emissions compared to the non-actuated operation. Furthermore, the present ultra-low-power NRPD-based control strategies

for sequential combustors opens other possibilities such as thermoacoustic instability control during transient operation by employing a feedback loop control.

4. Conclusions and outlook

This study demonstrates that ultra-low-power non-equilibrium plasma can effectively stabilize a thermoacoustically unstable sequential combustor. Indeed, the power of the plasma produced by the NRPD which can achieve thermoacoustic stabilization, can be 5 orders of magnitude lower compared to the flame thermal power: with a mean plasma power of 1.1 W, which is 1.5×10^{-3} percent of the flame thermal power of 73.4 kW, the thermoacoustic limit cycle in the sequential combustor was successfully stabilized. At this condition, there is practically no additional NO emission compared to the situation where the thermoacoustic mode was stabilized by changing the outlet orifice geometry of the combustor with a motor-driven water-cooled piston. However, at PRF = 40 kHz and generator voltages of 12.5 kV, and 13.2 kV, another thermoacoustic mode at 260 Hz becomes self-excited. Therefore, now that an effective ultra-low-power actuator has been found for sequential combustors in the form of NRPD in the sequential burner, a significant part of the research efforts should concentrate on the development of feedback control for ensuring optimum trade-off between global thermoacoustic stability and NO emissions during steady and transient operation. Finally, further investigations are required to demonstrate the practicality of this NRPD actuation at elevated pressures, and to develop predicting tools of the interaction between plasma kinetics and combustion reactions in the

thermochemical environment of the turbulent sequential burner.

Acknowledgements

This project has received funding from the European Research Council (ERC) under the European Union’s Horizon 2020 research and innovation program (grant agreement No [820091]).

References

- [1] A. Ciani, M. Bothien, B. Bunkute, J. Wood, G. Früchtel, Superior fuel and operational flexibility of sequential combustion in Ansaldo Energia gas turbines, *J. Glob. Power Propuls. Soc.* 3 (2019) 630–638.
- [2] D. A. Pennell, M. R. Bothien, A. Ciani, V. Granet, G. Singla, S. Thorpe, A. Wickstroem, K. Oumejjoud, M. Yaquinto, An introduction to the ansaldo GT36 constant pressure sequential combustor, *Proc. ASME Turbo Expo 4B* (2017).
- [3] M. R. Bothien, A. Ciani, J. P. Wood, G. Fruechtel, Sequential Combustion in Gas Turbines: The Key Technology for Burning High Hydrogen Contents With Low Emissions Volume 4A: Combustion, Fuels, and Emissions (2019).
- [4] R. Solana-Pérez, S. A. Shcherbanev, B. Dharmaputra, A. Ciani, N. Noiray, Combustion regime transition of h₂ flames during steady and transient operation of a sequential combustor, *P. Combust. Inst* (2022). <https://doi.org/10.1016/j.proci.2022.08.014>.

- [5] O. Schulz, N. Noiray, Combustion regimes in sequential combustors: Flame propagation and autoignition at elevated temperature and pressure, *Combust. Flame* 205 (2019) 253–268.
- [6] G. Bonciolini, N. Noiray, Synchronization of Thermoacoustic Modes in Sequential Combustors, *J. Eng. Gas. Turb. Power* 141 (2018).
- [7] T. C. Lieuwen, V. Yang, Combustion instabilities in gas turbine engines: operational experience, fundamental mechanisms and modeling, Vol. 210, 2005.
- [8] T. Poinsot, Prediction and control of combustion instabilities in real engines, *P. Combust. Inst* 36 (2017) 1–28.
- [9] L. Miniero, G. A. Mensah, C. Bourquard, N. Noiray, Failure of thermoacoustic instability control due to periodic hot gas ingestion in Helmholtz dampers, *J. Sound. Vib* 548 (2023) 117544.
- [10] M. Bothien, N. Noiray, B. Schuermans, A novel damping device for broadband attenuation of low-frequency combustion pulsations in gas turbines, *J. Eng. Gas. Turb. Power* 136 (2014) 041504.
- [11] S. Zahirovic, K. Knapp, Ansaldo GT26 Sequential Combustor Performance in Long-Term Commercial Operation, *Proceedings of the ASME Turbo Expo 4B* (2017) 64289.
- [12] N. Docquier, S. Candel, Combustion control and sensors: A review, *Progress in Energy and Combustion Science* 28 (2002) 107 – 150.

- [13] A. P. Dowling, A. S. Morgans, Feedback control of combustion oscillations, *Annu. Rev. Fluid. Mech* 37 (2005) 151–182.
- [14] M. R. Bothien, J. P. Moeck, C. O. Paschereit, Active control of the acoustic boundary conditions of combustion test rigs, *J. Sound. Vib* 318 (2008) 678 – 701.
- [15] J. Hermann, S. Gleis, D. Vortmeyer, Active instability control (aic) of spray combustors by modulation of the liquid fuel flow rate, *Combust. Sci. Technol.* 118 (1996) 1–25.
- [16] J. R. Seume, N. Vortmeyer, W. Krause, J. Hermann, C.-C. Hantschk, P. Zangl, S. Gleis, D. Vortmeyer, A. Orthmann, Application of active combustion instability control to a heavy duty gas turbine, *J. Eng. Gas. Turb. Power* 120 (1998) 721–726.
- [17] S. Starikovskaia, Plasma-assisted ignition and combustion: nanosecond discharges and development of kinetic mechanisms, *J. Phys. D. Appl. Phys* 47 (2014) 353001.
- [18] Y. Ju, W. Sun, Plasma assisted combustion: Dynamics and chemistry, *Prog. Energ. Combust* 48 (2015) 21–83.
- [19] A. Starikovskiy, Physics and chemistry of plasma-assisted combustion, *Philos. T. Roy. Soc. A* 373 (2015) 20150074.
- [20] I. V. Adamovich, W. R. Lempert, Challenges in understanding and predictive model development of plasma-assisted combustion, *Plasma. Phys. Contr. F* 57 (2014) 014001.

- [21] D. A. Lacoste, Flames with plasmas, *P. Combust. Inst* (2022).
<https://doi.org/10.1016/j.proci.2022.06.025>.
- [22] G. Pilla, D. Galley, D. A. Lacoste, F. Lacas, D. Veynante, C. O. Laux, Stabilization of a turbulent premixed flame using a nanosecond repetitively pulsed plasma, *IEEE. T. Plasma. Sci* 34 (2006) 2471–2477.
- [23] M. S. Bak, H. Do, M. G. Mungal, M. A. Cappelli, Plasma-assisted stabilization of laminar premixed methane/air flames around the lean flammability limit, *Combust. Flame* 159 (2012) 3128–3137.
- [24] R. Patel, J. van Oijen, N. Dam, S. Nijdam, Low-temperature filamentary plasma for ignition-stabilized combustion, *Combust. Flame* 247 (2023) 112501.
- [25] D. A. Lacoste, D. A. Xu, J. P. Moeck, C. O. Laux, Dynamic response of a weakly turbulent lean-premixed flame to nanosecond repetitively pulsed discharges, *P. Combust. Inst* 34 (2013) 3259–3266.
- [26] D. A. Lacoste, Y. Xiong, J. P. Moeck, S. H. Chung, W. L. Roberts, M. S. Cha, Transfer functions of laminar premixed flames subjected to forcing by acoustic waves, AC electric fields, and non-thermal plasma discharges, *P. Combust. Inst* 36 (2017) 4183–4192.
- [27] J. P. Moeck, D. A. Lacoste, C. O. Laux, C. O. Paschereit, Control of combustion dynamics in a swirl-stabilized combustor with nanosecond repetitively pulsed discharges, 51st AIAA Aerospace Sciences Meeting including the New Horizons Forum and Aerospace Exposition 2013 (2013) 1–11.

- [28] W. Kim, J. Cohen, Plasma-assisted combustor dynamics control at realistic gas turbine conditions, *Combust. Sci. Technol* 193 (2021) 869–888.
- [29] Y. Xiong, O. Schulz, C. Bourquard, M. Weilenmann, N. Noiray, Plasma enhanced auto-ignition in a sequential combustor, *P. Combust. Inst* 37 (2019) 5587–5594.
- [30] S. A. Shcherbanev, Q. Malé, B. Dharmaputra, R. Solana-Pérez, N. Noiray, Effect of plasma-flow coupling on the ignition enhancement with non-equilibrium plasma in a sequential combustor, *J. Phys. D. Appl. Phys* 55 (2022).
- [31] D. A. Lacoste, J. P. Moeck, D. Durox, C. O. Laux, T. Schuller, Effect of nanosecond repetitively pulsed discharges on the dynamics of a swirl-stabilized lean premixed flame, *J. Eng. Gas. Turb. Power* 135 (2013).
- [32] F. Di Sabatino, D. A. Lacoste, Enhancement of the lean stability and blow-off limits of methane-air swirl flames at elevated pressures by nanosecond repetitively pulsed discharges, *J. Phys. D. Appl. Phys* 53 (2020).
- [33] W. Kim, J. Snyder, J. Cohen, Plasma assisted combustor dynamics control, *P. Combust. Inst* 35 (2015) 3479–3486.
- [34] A. M. Alkhalifa, A. Alsalem, D. Del Cont-Bernard, D. A. Lacoste, Active control of thermoacoustic fluctuations by nanosecond repetitively pulsed glow discharges, *P. Combust. Inst* (2022). <https://doi.org/10.1016/j.proci.2022.06.013>.

- [35] N. Q. Minesi, V. P. Blanchard, E. Pannier, G. D. Stancu, C. O. Laux, Plasma-assisted combustion with nanosecond discharges. I: Discharge effects characterization in the burnt gases of a lean flame, *Plasma Sources. Sci. T* 31 (2022).
- [36] N. Noiray, A. Denisov, A method to identify thermoacoustic growth rates in combustion chambers from dynamic pressure time series, *P. Combust. Inst* 36 (2017) 3843–3850.
- [37] W. Kim, H. Do, M. G. Mungal, M. A. Cappelli, Flame stabilization enhancement and NOx production using ultra short repetitively pulsed plasma discharges, *Collection of Technical Papers - 44th AIAA Aerospace Sciences Meeting* 9 (2006) 6770–6772.
- [38] G. Bonciolini, A. Faure-Beaulieu, C. Bourquard, N. Noiray, Low order modelling of thermoacoustic instabilities and intermittency: Flame response delay and nonlinearity, *Combust. Flame* 226 (2021) 396–411.